Investigation into Nitrided Spur Gears

B.S. Yilbas, A. Coban, J. Nickel, M. Sunar, M. Sami, and B.J. Abdul Aleem

The cold forging method has been widely used in industry to produce machine parts. In general, gears are produced by shaping or hobbing. One of the shaping techniques is precision forging, which has several advantages over hobbing. In the present study, cold forging of spur gears from Ti-6Al-4V material is introduced. To improve the surface properties of the resulting gears, plasma nitriding was carried out. Nuclear reaction analysis was carried out to obtain the nitrogen concentration, while the micro-PIXE technique was used to determine the elemental distribution in the matrix after forging and nitriding processes. Scanning electron microscopy and x-ray powder diffraction were used to investigate the metallurgical changes and formation of nitride components in the surface region. Microhardness and friction tests were carried out to measure the hardness depth profile and friction coefficient at the surface. Finally, scoring failure tests were conducted to determine the rotational speed at which the gears failed. Three distinct regions were obtained in the nitride region, and at the initial stages of the scoring tests, failure in surface roughness was observed in the vicinity of the tip of the gear tooth. This occurred at a particular rotational speed and work input.

Keywords
plasma nitriding, spur gear

1. Introduction

THE COLD AND WARM forging of metals has gained importance due to the increasing demand for mass production of precision parts in industry. Depending on the temperature of the slug, the processes are called warm, hot, or cold forging (Ref 1). Warm forging may have several advantages, including better utilization of material, improved surface finish, and better dimensional accuracy when compared with hot forging, and reduced press loads when compared with cold forging (Ref 2). On the other hand, die-tool wear is considerable in warm forging. Alternatively, cold forging is a well-known process and is being developed continuously for producing geometries of ever-increasing complexity. It has been reported that cold forging produces parts with excellent tolerances and surface finish due to lack of the thermal expansion and scale formation found in hot forming (Ref 3). Consequently, postforging operations can be eliminated. However, cold forging is limited in terms of the shaping options and the choice of workpiece materials, because it results in relatively small deformation capability at room temperature. Therefore, in a multistage process the deformation capacity can be exhausted due to strain hardening before the intended operations have been completed. To overcome this problem, intermediate treatments such as annealing and phosphating have become necessary (Ref 4).

Gears are produced by either shaping or hobbing. To meet the high accuracy requirements and form complex geometric contours, several methods have been introduced and investigated: fine blanking, press shaving, roll forming, and precision forming. The requirements in these processes are low cost and finished-form end product. It has been suggested that fine blanking and press shaving are limited to a gear width of 6 mm (Ref 5) and that thicker gears can be produced through warm shaving. Roll forming has the disadvantages of low production rate and high cost (Ref 6). This process is also limited to ring gears. On the other hand, precision forging provides high accuracy, reduces row material disposal, and improves production time. However, due to the tool cost, precision cold forging of gears is not feasible for small-volume production (Ref 7). The multistage sequential method was applied by Korner and Knodler to form spur gears (Ref 8). The forming load was reduced considerably, but in some cases a further operation was required for the surface finish.

Ti-6Al-4V is an alloy that has been used extensively in industry due to its high strength and corrosion resistance at low specific weight. High friction coefficient and low wear resistance limit its widespread application, but many techniques are available to improve the tribological properties of the surface (Ref 9, 10). The formation of titanium nitride on the surface is one of the popular techniques for modifying the surface. Through the plasma nitriding process, considerable nitride layer thickness can be achieved (Ref 10).

The present study introduces cold forging of spur gears using a multiaction gear forming system. The gear materials selected was Ti-6Al-4V due to its high strength-to-weight ratio. In order to increase the wear properties of the spur gears produced, a plasma nitriding process was carried out (Ref 11). Two major methods of titanium nitriding can generally be applied: TiN molecules are formed in the gaseous phase and are then deposited on a substrate; or nitrogen atoms are allowed to diffuse into the titanium matrix. In the present study the second process was used to nitride the gear surfaces. Nuclear Reaction Analysis (NRA) and Particle Induced X-ray Emission (micro-PIXE) tests were conducted to determine the nitrogen concentration and elemental distribution in the vicinity of the surface of the gear material. The study was extended to include the investigation of the wear properties of the resulting gears.

2. Experiment

A multiaction cold forging system was used to form the gear samples. Forging was carried out in enclosed dies. Material

B.S. Yilbas,* A. Coban, J. Nickel,** M. Sunar,* M. Sami,*** and **B.J. Abdul Aleem,*** King Fahd University of Petroleum & Minerals, Dhahran 31261, Saudi Arabia
*Mechanical Engineering Department
**Energy Research Laboratory of the Research Institute

was led to flow from the lower punch side into the tooth-shaped cavity enclosed by the upper and lower dies. In the last stage, the stepped control mandrel was lifted gradually so that compression was gradually developed. With decrease in mandrel diameter, additional plastic flow was prompted, filling each tooth end cavity without any increase in compression force. The working stress caused in the sample was about 130 kgf/mm^2. Considerable small roll-over and burr around the teeth were observed. In the case of inner faces, machining of the bevel facing of the outer surface and grooving around the spherical surface were found to be unnecessary after forming. Figure 1 shows the resulting gear and its dimensions.

SOURCE OF VARIATION	Symbols	Units (mm)
Diametral pitch	P	0.35
Circular pitch	P_c	8.88
Pitch diameter	P_d	33.94
Outside diameter	D_o	39.59
Number of teeth in the gear	N	12
Tooth thickness	T	4.44
Addendum	a	2.83
Dedendum	b	3.27
Working depth	h_k	5.66
Whole depth	h_t	6.10
Clearance	S	0.44

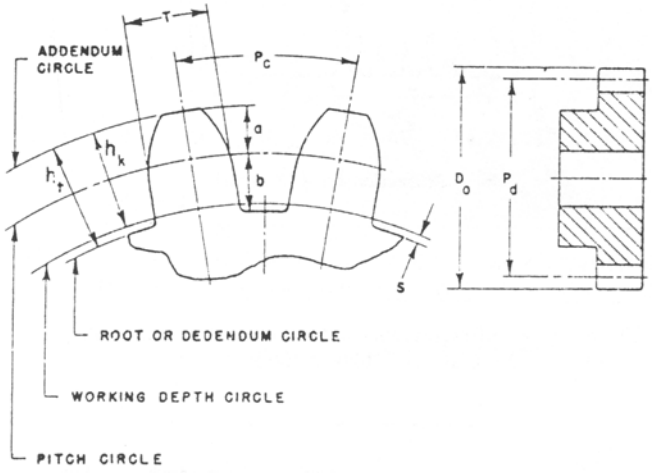

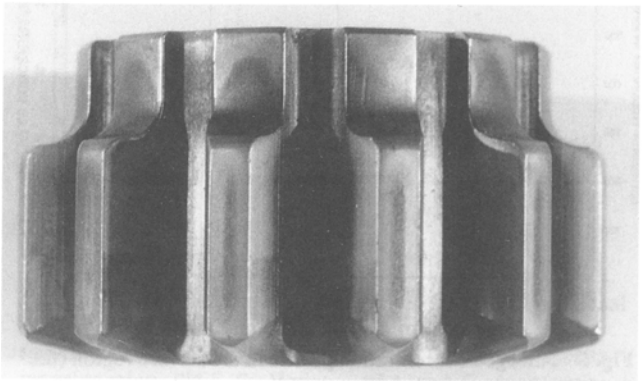

Fig. 1 Resulting gear and its dimensions

2.1 *Material and Plasma Nitriding Process*

The microstructure of the samples consists of α and β grains as shown in Fig. 2. The elemental weight percentages of the alloy are 6 Al, 4 V, 0.03 Cu, 0.01 Cr, 0.32 Fe, 0.2 O, and the balance Ti. The gear samples were degreased ultrasonically in acetone and dried in air. The samples were then placed in the nitriding unit, which operated within the direct current bias voltage range 400 to 700 V. Other nitridiing conditions were 520 °C, 54 to 72 ks, and 0.46 to 0.51 kPa total pressure. Prior to the nitriding process the gear samples were subjected to cleaning by sputtering in argon and hydrogen (3:1 ratio) plasma for 30 min. The nitriding was performed in an N_2-H_2 (8:1 ratio) plasma. The total volume flow rate varied between 40 and 120 cm^3/s. The temperature of the samples was kept at 520 °C during the nitriding process.

2.2 *NRA and micro-PIXE Tests for Nitrogen Depth Profile and Elemental Composition*

Nitrogen was analyzed using NRA at the Tandetron Accelerator of the Energy Research Laboratory (ERL) (Ref 12). The $^{15}N(p.\alpha\gamma)^{12}$ resonant reaction was used to profile nitrogen using the 430 keV resonance by detecting 4.43 MeV γ-rays with a NaI(Tl) detector. Measurements were carried out at different proton beam energies up to 830 keV. Nitrogen surface content was, however, measured at different parts of the gear at a proton energy of 905 keV (i.e., using the 898 keV high cross section resonance of this reaction). Measurements were compared with a TiN standard produced by a physical vapor deposition technique on a Ti-6Al-4V alloy. The micro-PIXE measurements were conducted to determine the titanium, aluminum, and vanadium one- and two-dimensional distributions using the ERL nuclear microprobe with a spatial resolution of about 5 × 5 μm^2 (Ref 13).

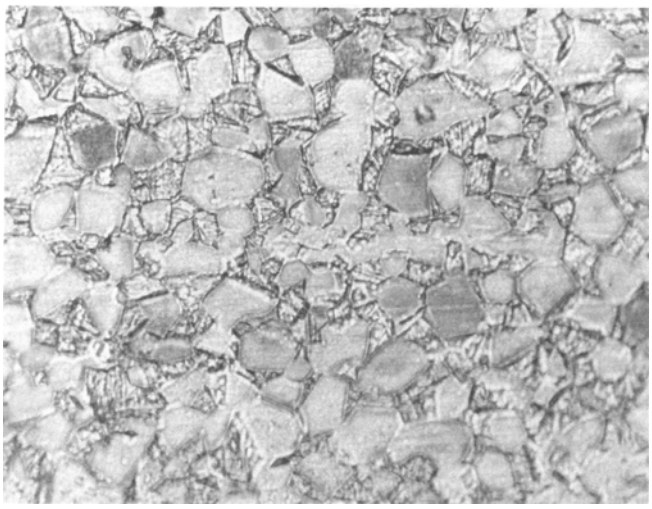

Fig. 2 Microphotograph of Ti-6Al-4V sample showing α and intergranular β

2.3 *Scoring Failure Tests*

The failure tests were conducted on gear pairs of which the pinion and wheel had the same nitridings. The tests were carried out according to the international standards (Ref 14). The gears tests were lubricated with an oil with viscosity of 30×10^{-6} m^2/s at 40 °C. The oil was flashed onto the meshing faces at a rate of 0.003 m^3/s. The oil temperature was kept constant at 40 °C. A circulating gear setup was used to provide a variable rotational speed of the pinion. The rotational speed was set at 1800 rpm at the beginning and increased to 8500 rpm in increments of 250 rpm. The load applied per unit face width varied from 250 to 400 N/mm. The load was increased in increments of 25 N/mm when no scoring failure was obtained at the highest speed, 8500 rpm. The tests were conducted until the total number of pinion revolutions reached 10^5. The scoring was based on surface roughness measurements along the tooth trace.

2.4 *Friction and Microhardness Tests*

To measure the friction coefficient, a ball-on-disc machine was used for all tests. The ball material was hardened AISI 52100 steel that was allowed to slide, dry, on a sample rotating at 100 rpm under a load of 1 N. The friction force was measured during sliding as a function of time. At the time of breakthrough, the friction increased drastically and showed critical behavior thereafter, indicating scuffing-like wear characteristics. Microhardness tests were carried out using microhardness equipment. Specimens were cut in section, ground, and polished before the measurement. The microhardness measurements were taken across the nitrided surfaces.

2.5 *XRD Microphotography*

The nitrided layers were analyzed using x-ray powder diffraction (XRD) that employed CuK_α and MoK_α radiation. The lattice parameters were calculated from the diffractagrams obtained with CuK_α radiation, and the error relevant to measurement of the lattice was ±0.6 Å. Scanning electron microscopy (SEM) was used to obtain microphotographs of tooth cross sections after the nitriding process. In addition, microphotography

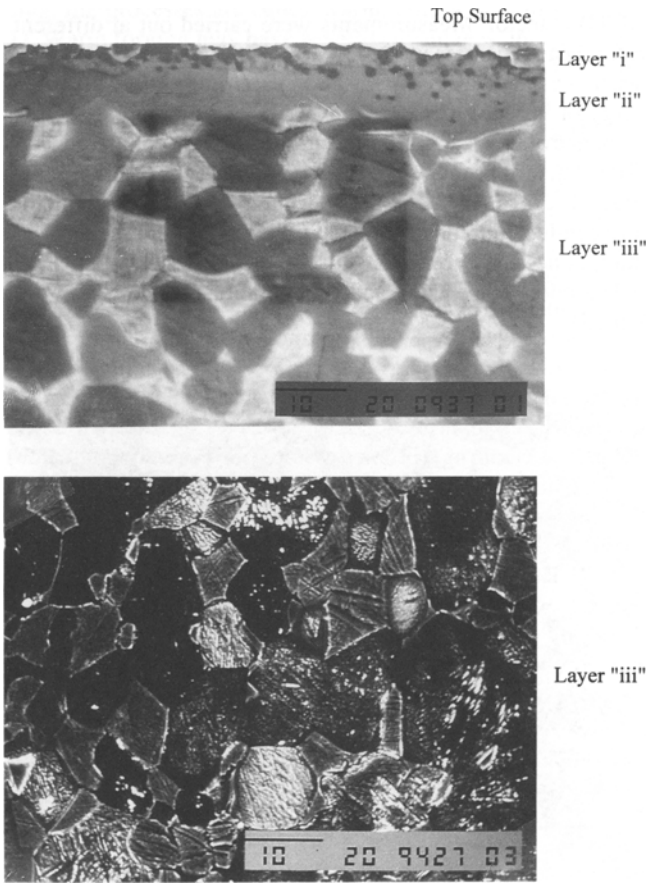

Fig. 3 SEM microscopy photographs cut from a sample that was nitrided for 54 ks at 520 °C at a D.C. bias of 700 V

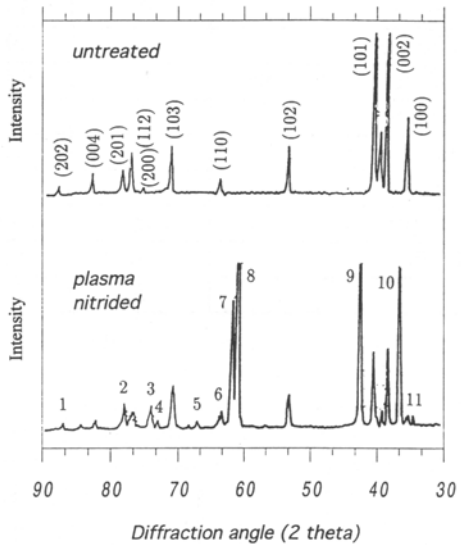

1	2	3	4	5	6	7	8	9	10	11
ε-Ti_2N (302)	δ-TiN (222)	δ-TiN (311)	ε-Ti_2N (202)	ε-Ti_2N (311)	ε-Ti_2N (102)	δ-TiN (220)	ε-Ti_2N (002)	δ-TiN (200)	δ-TiN (111)	ε-Ti_2N (101)

Fig. 4 X-ray diffractograms of the surface of a sample nitrided for 54 ks at 520 °C at a D.C. bias of 700 V

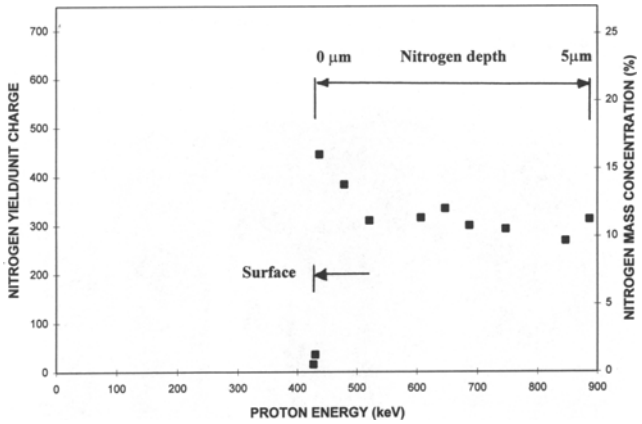

Fig. 5 Nitrogen concentration profile in the surface region (the depth of nitrogen profile will extend further). Sample is nitrided for 54 ks at 520 °C at a D.C. bias of 700 V

was conducted across the tooth surfaces after the scoring failure tests were completed.

3. Results and Discussion

3.1 *Microphotography and XRD Results*

It was evident from visual inspection of samples that a short nitriding time resulted in a bright yellow surface. When nitriding time increased, the surface changed to a bright golden color. As the surface temperature increased during the nitriding process, the surface turned a darker color. This occurred at 30 h of nitriding and 550 °C nitriding temperature. SEM photographs of sample cross sections are shown in Fig. 3. The nitrided zone is composed of three layers. The interface between the compound layer (layer i) and the inner layer (ii) is sharp, while the interface between the inner layer and the outer layer (layer iii) is diffuse. These layers have thicknesses of 10, 15, and 40 μm, respectively, and they are composed of different nitride phases. It is evident from XRD results (Fig. 4) that δ-TiN and ε-Ti_2N phases exist in the nitrided layer. In the component layer, δ-TiN + ε-Ti_2N phases occur, while α-TiN phase with or without ε-Ti_2N phase occurs in the inner layer. In the outer layer, nitride precipitates are distributed evenly close to the intermediate layer.

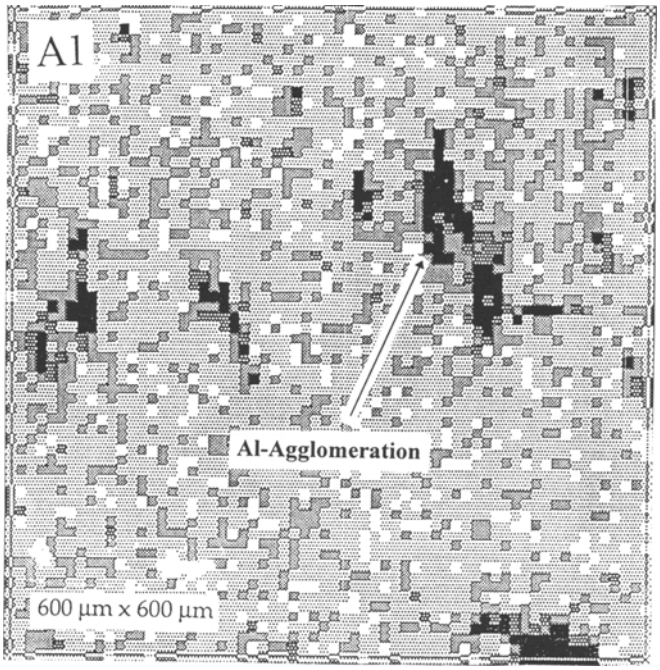

(a)

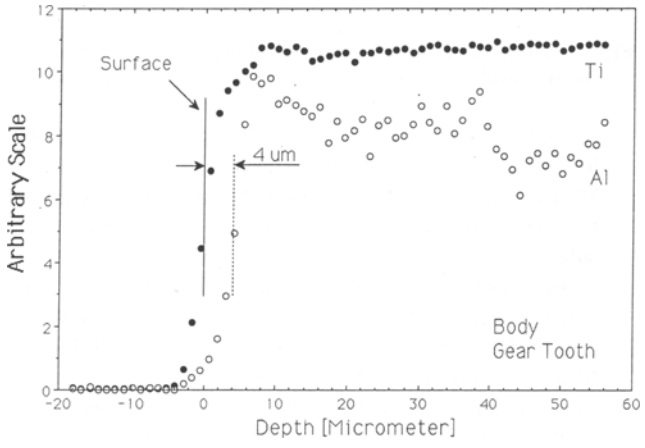

(b)

Fig. 6 Aluminum surface agglomeration. (a) Two-dimensional Al elemental distribution in the vicinity of tooth surface. This two-dimensional map was obtained on the Tandetron Accelerator using micro-PIXE. (b) Variation of Al and Ti concentration in the tooth cross section

3.2 *NRA and micro-PIXE Results*

The nitrogen concentration at inner surfaces of the gears was lower than at outer surfaces (nitrogen mass concentration at the inner surface is about 12%, but at the outer surface about 17%). This may be due to the glow discharge developed during the nitriding process (in this case, the gas pressure in the nitriding chamber is considerably lower). However, as this gas pressure increases, plasma becomes more dense, plasma current increases, and more plasma reaches the inner surface, so the nitrogen concentration is expected to increase (Ref 15). As the plasma gas pressure increases, abnormal glow discharge develops, leading to a high risk of arc formation. Nevertheless, the nitrogen concentration provides useful information to serve the present purpose.

Figure 5 shows the mass concentration of nitrogen with distance from the surface of the tooth, obtained from NRA measurement. It is evident that a nitrogen mass concentration of 17% is obtained in the vicinity of the surface. The nitrogen depth profile measurement is limited by the characteristic of the nuclear reaction employed, so it is expected that the nitrogen mass concentration will extend farther inside the material.

Figure 6 shows the two-dimensional map of aluminum and the concentration of the aluminum corresponding to the gear tooth. It can be seen that deficiency in aluminum concentration

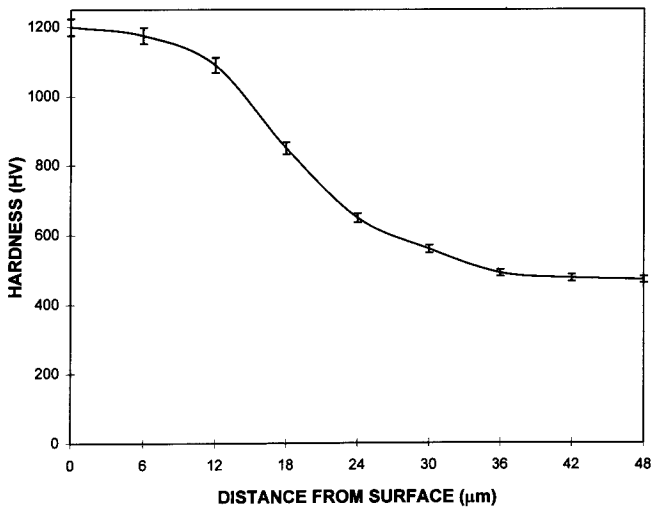

Fig. 7 Microhardness test results. Treatment is for 54 ks at 520 °C at a D.C. bias of 700 V

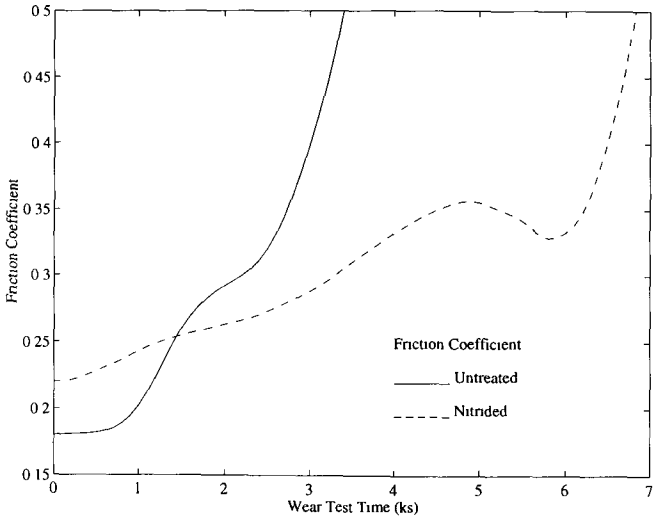

Fig. 8 Friction test results from ball-on-disc set-up. Applied load is 1 N and sample rotation is 100 rpm

occurs in the vicinity of the free surface of the tooth. In addition, a local aluminum agglomeration is evident.

3.3 *Friction and Microhardness Test Results*

The microhardness across the nitride surface is shown in Fig. 7. The microhardness decreases with increasing distance from the surface. Friction test results are shown in Fig. 8. The effect of plasma nitriding can be clearly seen. For the untreated samples, severe scuffing-like wear occurred on the surface after only a few wear cycles. The friction coefficient, after being relatively constant for a period at the start of the test, increased abruptly before breakthrough occurred.

3.4 *Scoring Failure Test Results*

Figure 9 shows the surface roughness variation along the tooth at the meshing faces of the pinion. The variation is relatively small for the speed range of 1800 to 2500 rpm. As the rotational speed increased to 6000 rpm, a scoring failure occurred at the double tooth contact zone on the side of the root of the pinion. With respect to wheel surface roughness, a surface failure due to scoring was observed in the vicinity of the tip at the initial stage of scoring for the gear pairs. Figure 10 shows the rms values of surface roughness along the tooth trace at the meshing faces, with work input per unit face width. The surface roughness measured in the vicinity of the tooth surface indicates that scoring failure occurs. It is also evident that the scoring failure occurs at an energy input of 35 MJ/mm and at 6000 rpm rotational speed.

4. Conclusions

- Three distinct regions developed in the nitrided layer: δ-TiN + ε-Ti_2N, α-TiN with or without ε-Ti_2N, and unevenly distributed nitride precipitates.
- Some deficiency in the nitrogen distribution across the tooth occurs (i.e., nitrogen concentration at the tooth surface varies). This variation is due to the nitriding process.

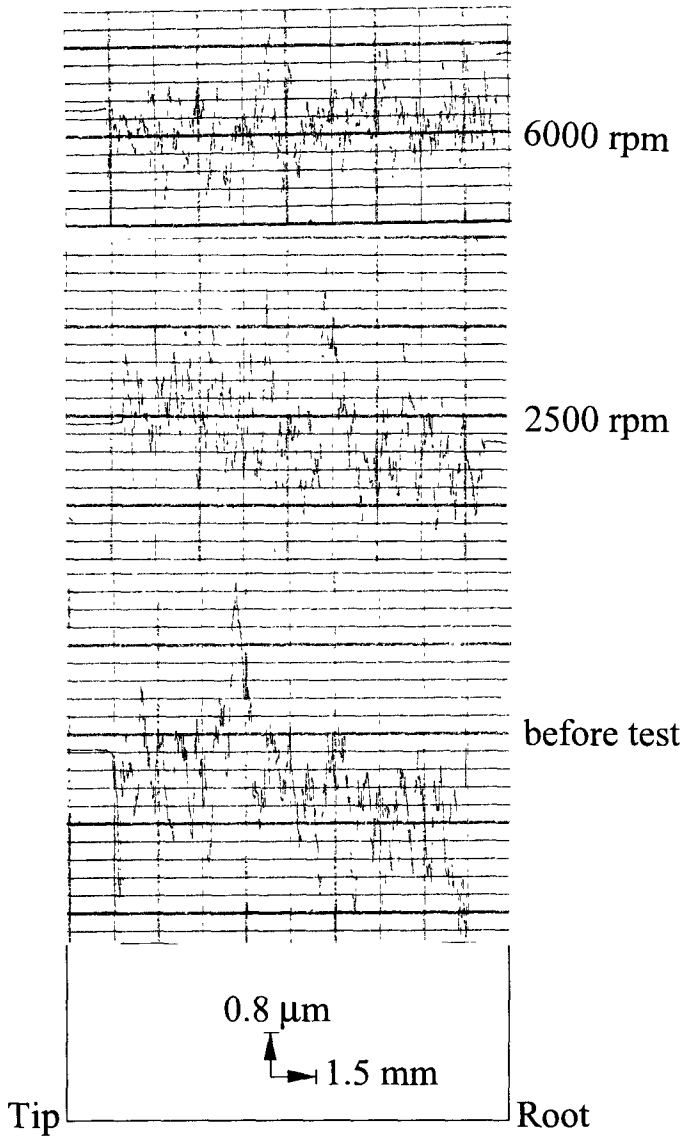

Fig. 9 Variation in surface roughness along tooth of meshing of pinion. Nitriding is for 54 ks at 520 °C at a D.C. bias of 700 V

Nevertheless, this variation is small and is expected to have little effect on the surface wear properties.

- Microhardness test results show that the hardness profile follows the nitride profile developed in the vicinity of the substance surface. The friction test results indicate that untreated samples suffer severe scuffing-like wear after a few wear cycles. The friction coefficient of the nitrided surfaces is almost constant for some time and increases abruptly before the occurrence of breakthrough.
- The aluminum concentration in the matrix decreases at the tooth surface about 90% from that in the matrix. This may be due to the plasma nitriding process. In addition, a local aluminum agglomeration occurs in the vicinity of the surface.
- From the initial results, surface failure due to scoring is evident in the vicinity of the tip of the tooth. The scoring failure occurs at a work input of 22 MJ/mm and at 6000 rpm rotational speed.

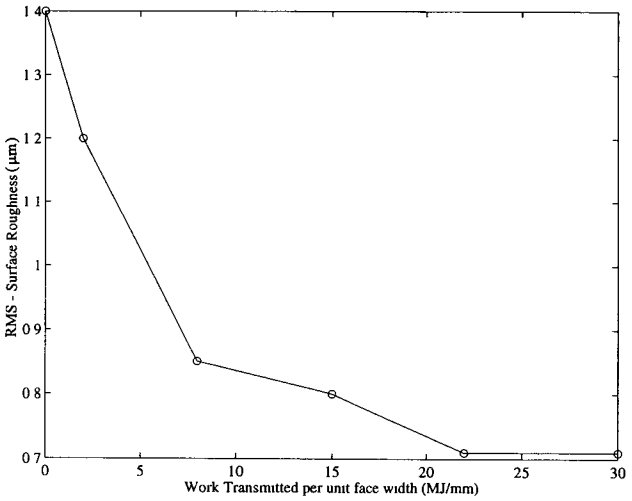

Fig. 10 Variation in surface roughness along tooth profile at meshing faces of pinion

Acknowledgments

The authors would like to acknowledge the support of the Energy Research Laboratory of the Research Institute, King Fahd University of Petroleum & Minerals.

References

1. R. Shivpuri, S. Babu, S. Kini, P. Pauskar, and A. Deshpande, Recent Advances in Cold and Warm Forging Process Modelling Techniques: Selected Examples, *J. Mater. Process. Technol.*, Vol 46, 1994, p 253-274
2. S. Sheljaskov, Warm Forging in Comparison with Hot and Cold Forging, *Proc. Fourth ICTP*, (Beijing), Sept 1993, p 1082-1087
3. S. Sheljaskov, Current Level of Development of Warm Forging Technology, *J. Mater. Process Technol.*, Vol 46, 1994, p 3-18
4. M. Hirschvogel and H.V. Doolen, Some Applications of Cold and Warm Forging, *J. Mater. Process. Technol.*, Vol 35, 1992, p 343-356
5. H. Kudo, Towards Net-Shape Forming, *J. Mater. Process. Technol.*, Vol 22, 1990, p 311-342
6. M.H. Sadeghi and T.A. Dean, Precision Forging Straight and Helical Spur Gears, *J. Mater. Process. Technol.*, Vol 45, 1994, p 25-30
7. S. Fujikawa, H. Yoshioka, and S. Shimamura, Cold and Warm-Forging Applications in Automotive Industry, *J. Mater. Process. Technol.*, Vol 35, 1992, p 317-342
8. E. Korner and R. Knodler, Possibilities of Warm Extrusion in Combination with Cold Extrusion, *J. Mater. Process. Technol.*, Vol 35, 1992, p 451-468
9. A. Gicquel, N. Laidani, P. Saillard, and J. Amouraux, Plasma and Nitrides: Application to the Nitriding of Titanium, *Pure and Appl. Chem.*, Vol 62 (No. 9), 1990, p 1743-1750
10. N. Laidani, J. Perriere, D. Lincot, A. Gicquel, and J. Amouraux, Nitriding of Bulk Titanium and Titanium Films in a NH_3 Low Pressure Plasma, *Appl. Surf. Sci.*, Vol 36, 1989, p 520-529
11. A. Leyland, K.S. Fancey, A.S. James, and A. Matthews, Enhanced Plasma Nitriding at Low Pressures: A Comparative Study of d.c. and r.f. Techniques, *Surf. Coat. Technol.*, Vol 41, 1990, p 295-304
12. A. Coban, J. Nickel, and M.A. Garwan, "Nuclear Reaction Analysis at KFUPM," paper presented at the 13th Int. Conf. on the Applications of Accelerators in Research and Industry (Denton, TX), 7-10 Nov 1994
13. M. Ahmed, J. Nickel, A.B. Hallak, R.E. Abdel-Aal, A. Coban, and H.A. Al-Juwair, The KFUPM Scanning Nuclear Probe Facilities, *Nuclear Instruments and Methods in Physics Research*, Vol B82, 1993, p 584-588
14. ISO/TC 60/WG 6, Netherlands, 17, "Calculations of Scoring Resistance of Gear Drives," 1975
15. R. Grun and H.-J. Gunther, Plasma Nitriding in Industry—Problems, New Solutions and Limits, *Mater. Sci. Eng.*, Vol A140, 1991, p 435-441